THE TOTAL NEUTRON CROSS-SECTION OF PALLADIUM USING THE M.I.T. FAST CHOPPER

by

PAUL JEROME SCHWEITZER

MALVIN CARL TEICH

SUBMITTED IN PARTIAL FULFILLMENT OF THE
REQUIREMENTS FOR THE DEGREE OF
BACHELOR OF SCIENCE

at the

MASSACHUSETTS INSTITUTE OF TECHNOLOGY

June, 1961

Signature of Authors . . . . . .
Department of Physics, June, 1961

Certified by . . . . . .
Thesis Supervisor

Accepted by. . . . . .
Chairman, Departmental Committee on Theses

THE TOTAL NEUTRON CROSS-SECTION OF PALLADIUM USING THE M.I.T. FAST CHOPPER

by

PAUL JEROME SCHWEITZER

MALVIN CARL TEICH

Submitted in Partial Fulfillment of the Requirements for the Degree of Bachelor of Science at the Massachusetts Institute of Technology, June, 1961.

ABSTRACT

Transmission experiments have been made to determine the total neutron cross-section of Palladium from 0.07 to 10 e.v. with a resolution of 0.43 μsec/m. The construction and performance characteristics of the fast chopper and the time-of-flight equipment at the M.I.T. reactor are briefly described. A new resonance of 14.3 ± 1.6 barns was located at 2.97 e.v.

Thesis Supervisor — Theos J. Thompson

Title — Professor of Nuclear Engineering

ACKNOWLEDGEMENT

It is a pleasure to thank Professor Theos J. Thompson, Director of the M.I.T. Nuclear Reactor, for his encouragement and continued support without which this project could not have been possible. The authors are indebted to Carl A. Anderson, Jr., who did much of the work in preparing the chopper setup for time-of-flight and spectrum work, for his helpful suggestions and valuable assistance during the course of the investigation.

This work was done in part at the M.I.T. Computation Center, and the aid received there is acknowledged.

Gratitude is expressed to Professor Norman C. Rasmussen for his able advice, to Professor William H. Dennen and the Cabot Spectrographic Laboratory, to F. Woodworth and the M.I.T.R. Machine Shop, and to D. Lynch and the M.I.T.R. Electronics Shop.

TABLE OF CONTENTS

SECTION I

INTRODUCTION

While much information is available for the low-lying energy levels of many nuclides, information relating to the excitation energies near the nucleon binding energy is not readily available. Neutron cross-section data has afforded an opportunity of experimentally determining the properties of the nuclear energy levels just above the neutron binding energy which is of the order of 7 Mev, and then correlating these results with theoretical predictions based on various models.

Either crystal spectrometers or time-of-flight apparatus may be used in measuring total neutron cross-sections. A figure of merit for time-of-flight measurement is the resolution, given in microseconds per meter (μsec/m), which is proportional to the uncertainty in the measurement of the neutron energy.

The primary objective of this investigation has been the measurement of the total neutron cross-section of palladium in the energy range 0.1 - 10.0 e.v., and the determination of the location of any low-lying resonances. These measurements were effected by conventional transmission experiments using palladium metal foils.

Such data have been incomplete in the past[1] due to the almost exclusive use of fast neutron choppers in higher

energy ranges, although they are equally as valuable in the energy range with which we are concerned.

SECTION II

DESCRIPTION OF APPARATUS

A schematic diagram of the fast chopper and associated time-of-flight apparatus is shown in Figure 1. Photographs of the experimental arrangement are included for clarity. The equipment is located at 12SN1, the 12" horizontal port at the M.I.T. Nuclear Reactor.

Reactor

The thermal flux at the base of the reactor port is approximately 5×10^{12} neutrons/cm^2-sec while the epithermal flux, which is of interest to us, obeys the dE/E spectrum. A collimator located within the port produces a well-defined neutron beam which then enters the chopper, mounted flush with the reactor wall.

Power Monitor

A Nancy-Wood counter is imbedded in the Masonite which holds the collimator. This counter serves to trigger a separate scaler, the power monitor, whose output is proportional to the total number of neutrons entering the chopper.

The chopper was built by the Christen Michelsens Institutt at Bergen, Norway. It has been described in detail elsewhere[2] and our discussion will therefore be limited to the more salient features of its operation. The chopper has

a 49 cm. diameter lucite rotor with 8 slits which rotates in a 2 mm. Hg vacuum at frequencies ranging from 100 to 8000 rpm. A feedback mechanism maintains a constant rotor speed to within 1 percent at a rotor speed of 3000 rpm.

The transmission of neutrons through the rotor is a function of both neutron energy and rotor speed. A theoretical plot of the rotor transmission has been obtained[2] and is illustrated in Figure 2. The reader's attention is called to the low-energy cutoff of the curve which, in conjunction with a sufficiently small flight path, prevents secondary neutrons* from being counted.

A light pulse traversing the same path through the rotor as the neutrons, and detected by a photomultiplier system, signals the beginning of a neutron burst.

Flight Path

The neutrons travel in a polyethylene drift-tube which is filled with helium at atmospheric pressure, and which serves to reduce air-scattering. The flight path is 25.835 meters long, and takes the neutrons from the chopper, through a one-half inch aluminum window which is part of the outer reactor wall, to the detector bank.

---

*Secondary neutrons are fast neutrons which have overtaken the slower neutrons of the previous burst.

Detectors

The neutron detection system consists of twenty enriched Reuter-Stokes $B^{10}F_3$ proportional counters, each tube twenty inches long and one inch in diameter, arranged in four rows of five tubes each. They are at a pressure of 167 cm. Hg, and their outputs are connected in parallel through an amplifier to the multi-channel analyzer.

The detector efficiency obeys the well known 1/v law, and is approximately 1 percent for 1 Kev. neutrons. Experiments have shown that the BF_3 tubes are comparatively insensitive to gamma-rays, and considerable boral and boron carbide shielding surrounds the detectors in order to minimize the effect of stray radiation.

The 4" thickness of the tubes in the beam direction, superimposed upon the 1/2" uncertainty in the length of the drift-tube gives a combined 2" uncertainty in the length of the flight-path. (See Section III and Appendix IV for discussion of longitudinal length-of-flight and longitudinal time-of-flight uncertainties). The difference in time-of-flight to various transverse parts of the BF_3 bank is negligible in comparison with longitudinal timing uncertainties at the energies of concern; consequently no corrections are made for it. (See Appendix IV).

Multi-Channel Analyzer

The multi-channel analyzer, (manufactured by the

Technical Measurements Corporation, model CN110, logic unit 211), records the pulses from the detectors in 256 equal-time channels. Delays of zero to three cycle times can be used, and channel widths which may be varied by factors of 2 from 0.25 to 64 usec. are available, and are constant to one part in 20,000, according to the manufacturer. The correction for deadtime counting losses for this apparatus is found in Appendix I.

The output of the analyzer is printed on tape and is then converted to punched-cards for processing on the IBM 709 computer at M.I.T. The program of data analysis is found in Appendix II and will be discussed in Appendix III.

SECTION III

PERFORMANCE CHARACTERISTICS

Burst-Shape

The burst-shape* can be determined by the static measurement of count rate as a function of the angular position of the rotor. Its expected shape is triangular[3], and a duty-cycle conversion gives the burst-shape for any given number of revolutions per minute of the rotor, f. The full burst-width was found from the ratio of the rotor slit width, w, to the circumference of the rotor, $2\pi R$, by using the relationship:

$$\Delta t = w/2\pi Rf \qquad (3.1)$$

The full burst-width at half-maximum will be just one-half of this value.

Time Calibration

By means of the known nuclide resonances discussed in the next part of this section, it has been ascertained that no linear displacement of the channels occurs, that is channel number 2 indeed records the infinite-velocity neutrons.+

---

*Plot of the relative number of neutrons leaving the rotor-slit versus rotor-slit position

+Channel Number 1 records no counts.

Timing Uncertainties

Four independent factors, the collection time of the detectors and associated electronics, the burst shape, the detector length, and the channel-width, contribute to the overall uncertainty in the neutron time-of-flight.

Collection time is comprised of the jitter time of the neutron detectors and the response time of the electronics. The jitter time of the BF_3 tubes has been measured to be 1/2 μsec. The agreement between the calculated and experimentally observed channel location of known resonances in In, Cd, and Au, showed that the combined collection time and photomultiplier delay time is less than 4 μsec.

The finite burst-width results in an uncertainty in the time at which the neutron leaves the chopper rotor. The probability distribution of departure time is proportional to the burst shape, and is therefore triangular with width inversely proportional to rotor frequency, as discussed in the first part of this section.

The probability of neutron capture within the detectors is a function of neutron energy and distance traveled. In Appendix IV it is concluded that, in the energy range of interest, the average capture time is approximately one-half of the time required to traverse the detector bank while the standard deviation is three-fourths of this time. The average length of detector traveled

before capture is therefore one-half of the tube length, with one standard deviation being three-fourths of this length. These conclusions justify the measurement of flight path to the center of the detector bank, with a detector length uncertainty of 1 1/2".

Channel widths were chosen to be comparable in size with the largest of the above three time uncertainties. The burst-width is the principle source of time uncertainty* for our chopper.

The overall time uncertainty Δt may be computed from the formula

$$\Delta t = \sqrt{(\Delta t_1)^2 + (\Delta t_2)^2 + (\Delta t_3)^2 + (\Delta t_4)^2} \qquad (3.2)$$

where Δt_1, Δt_2, Δt_3, and Δt_4 are respectively collection time, full burst width at half-maximum, standard deviation of capture time, and channel width. It is a function of both rotor speed and neutron energy. The instrument resolution $\Delta (t/\ell) \simeq \Delta t/\ell$ where ℓ is the length of flight path, will also depend on these same variables.

Resolution Function

The probability distributions for the burst-width and capture time have already been cited. If the collection

*For example, the 5.5 μsec. uncertainty at .1 e.v. due to detector length is negligible in comparison with the 28 μsec. burst-width at this energy (rotor speed of 850 r.p.m.).
See page 45.

and recording of neutrons are assumed equiprobable over the collection time and channel width, the four probability curves may be convoluted* to obtain the resolution function R(t) of the apparatus as a whole. R(t)dt is then the probability that a neutron of fixed energy is recorded by the analyzer between times t and t + dt later than the average time that a neutron of this energy is recorded, and can be used to correct the observed transmission for so-called time-smearing effects.

Background

It is found that there is a certain amount of background, that is, spurious counts arising from sources other than the neutron beam under consideration. These counts are automatically included in the count-rates obtained from the equipment and must be subtracted to give a true count value. The background counts are generally considered in two independent classes: the time-independent background and the time-dependent background. One method of measurement of total background counts involves intercepting the beam by means of a sample with a known strong resonance and of sufficient thickness to attenuate the direct beam completely. The time-dependent background may be obtained, if desired,

---

*Proof that the sum of several independent random variables has a probability distribution which is the convolution of the probability distributions of its components is found in H. Cramer, The Elements of Probability Theory, John Wiley and Sons, New York (1955) for the case of two variables. For the many variable case, an inductive proof based upon the associative property of the convolution operation may be employed.

by intercepting the beam with a polyethylene block, and subtracting these counts from the above result. Time-dependent background was found to be negligible. The background count rates are tabulated for convenience in Table 1.

Count-Rate

If the number of counts recorded in any channel of the multichannel analyzer is N, a one standard deviation uncertainty in N is given by $\sqrt{N}$; the fractional error is then $1/\sqrt{N}$. This uncertainty in the number of counts must be taken into account in evaluating the resolution and is explained in Appendix III.

The relationship between the number of counts in the various channels can be obtained by considering the epithermal spectrum. This flux is detected by a 1/v detector and, provided that the channels are all of equal time length, results in a constant number of counts in all channels.* This conclusion must be modified by the energy dependence of the rotor transmission; in practice, the experimental open beam count rate versus energy curve is used to determine the shape of the rotor transmission function.

The dependence of total count rate on rotor speed and channel width can be seen from Table 1. Calculations

---

*The spectrum impinging upon the detector is dE/E. Therefore the count-rate is proportional to $dE/E^{3/2}$ dt, and for constant dt, i.e., constant channel-width, the count rate is constant.

show that approximately 1/4 neutron per burst is observed. The number of neutrons per burst increases with decreasing rotor speed because of both the neutron energy spectrum and the rotor transmission function. In all runs the channel widths chosen resulted in analyzer operation during approximately 80 percent of the time between bursts.

SECTION IV

CROSS SECTION MEASUREMENT

Transmission Determination of Cross-Section

The total neutron cross section, σ_T, is evaluated from the relationship

$$\sigma_T = - \frac{\ln T}{nt} \qquad (4.1)$$

where n is the number of atoms per unit volume and t is the thickness of the sample under investigation.* The transmission, T, is the experimentally determined ratio of the sample-intercepted to open beam neutron intensities. It may be measured as a function of the incident neutron energy and from this measurement, the behavior of σ_T as a function of the neutron energy can be inferred. Because the measurement of total cross-section is performed by means of a transmission experiment, utilizing a ratio of intensities, no knowledge of transmission through the chopper, transmission through the drift tube, energy dependence of the counters and other constants of a given run is necessary. The only requirement is that these factors remain the same during both the open and sample-intercepted runs of each experiment.

---

*The derivation of the above formula can be found in Evans, The Atomic Nucleus. It does not, however, account for many of the considerations which are taken up in the following section.

Chopper Rotor Frequency

As a consequence of the above discussion, minor variations in the speed of the chopper rotor do not affect the measurement of cross-section provided that the average rotor speed remains constant. The rotor speed itself need not be known for obtaining the cross-section, rather it is chosen as a compromise between the following two conditions:

(1) The rotor speed must be sufficiently low such that a satisfactorily large number of neutrons in the energy range of interest are transmitted by the rotor (See Figure 2). This is necessary for good counting statistics and low cross section error, $\Delta\sigma_T$.

(2) The rotor must rotate rapidly enough to permit a small burst width. This provides for good time-resolution and a small error in the energy, $\Delta E/E$.

With our equipment, it was found that the optimum rotor speed for making measurements in the energy range 1.0 to 10.0 e.v. is 3000 r.p.m. In the energy range 0.1 to 1.0 e.v., this optimum speed is 850 r.p.m.

Computer Program

A Fortran program was written for the IBM 709 digital computer to mechanically perform the calculation of transmission and cross-section, as functions of the energy, and to indicate bracketing values of one standard deviation for all of the above parameters.

The programmed input to the computer consists of punched cards containing numerical values of the intensity of the open and sample-intercepted beams, constants of the run, and error corrections. This is a convenient method of data-analysis for cross-section investigations and the program is therefore appended for reference.

Sample

The element Palladium was chosen for investigation since its cross-section has not previously been determined in the energy range 0.1 to 10.0 e.v. The metallic samples were supplied by a metallurgical firm and were guaranteed by the rolling-mill to be 99.97 percent pure, with all impurities in the platinum metal family. This insured that any impurity would introduce a negligible error to the cross-section of palladium itself because of the nature of the cross-section of the platinum family in the energy range of concern. (See Appendix V). A spectroscopic analysis of the sample completely verified these conclusions. It is included in Appendix V for reference.

Each sample dimension was found to be uniform to within 0.1 percent in size; micrometer readings were taken at intervals along the plate and were found to agree to within one percent with the thickness obtained from area and weight measurements.

The sample is secured in its holder, which is situated in a slit in the inlet collimator inside the reactor port, intercepting the neutron beam before it arrives at the chopper. This provides for complete interruption of the beam with a relatively small sample.

Sample Thickness

The sample thickness was chosen to allow the most accurate determination of the cross-section σ_T in the running time available.

The equation for the percentage uncertainty in σ (See Appendix III),

$$\frac{\Delta\sigma}{\sigma} = \frac{\sqrt{\left(\frac{\Delta N}{N}\right)^2 + \left(\frac{\Delta N_\circ}{N_\circ}\right)^2}}{n\sigma t} = \frac{\sqrt{\frac{1}{N} + \frac{1}{N_\circ}}}{n\sigma t} \qquad (4.2)$$

indicates that a high count-rate and a thick sample are desirable for a low value of $\Delta\sigma/\sigma$. However, a high count-rate requires a high transmission and this is possible only with a thin sample. These two conflicting arguments dictate an intermediate choice of sample thickness, chosen to provide a transmission of 0.60. This value of T guarantees both a reasonably high count-rate and a moderate thickness. Because the cross-section increases at resonance, a smaller value of thickness is necessary there to maintain a high transmission.

For this reason, two sample thicknesses of Palladium were employed in measuring σ_T in the energy range

of interest. First, a run was made with the thick sample to provide a survey of the unknown energy range. Then, upon finding the approximate magnitude of a new resonance, another sweep of the energy range was made with a thinner sample, whose thickness is found from the criterion of constant transmission as indicated above.

Transmission data were collected over a period of from one to ten hours and it was found that samples of two different thicknesses provided the accuracy desired in the region examined.

SECTION V

CROSS-SECTION DETERMINATION

Correction for Variable Reactor Power

The transmission T is defined as the ratio of counting rates with and without sample in the beam only when the incident beam is constant during both runs. But, the ratio of neutrons emerging from the foil to neutrons incident upon it is of actual interest for cross-section determination. Since the power monitor output is proportional to the total number of neutrons incident upon it, the transmission can be more generally defined as

$$T = \frac{N}{N_\circ} \frac{P_\circ}{P} \qquad (5.1)$$

where $\frac{N}{N_\circ}$ is the ratio of total counts received during the two runs and $P_\circ/P$ is the ratio of power monitor readings during the same two runs. By use of Equation (5.1), no detailed knowledge of reactor power fluctuations is necessary.

Corrections to the Observed Counting Rate

The counts N and $N_\circ$ during the sample-intercepted and open-beam runs used in Equation (5.1) must be counts due to neutrons impinging on the sample and to no other causes. These numbers may be obtained by applying the following two corrections to the counts recorded by the analyzer:

Dead-time counting losses are corrected for Equation (A1.5) which gives the true number of counts N' and $N'_\bullet$ recorded by the neutron detectors. Background counts B must then be subtracted from the above leaving counts due only to those neutrons passing through the sample. Equation (5.1) then reduces to

$$T = \frac{N' - B}{N'_\bullet - B} \quad \frac{P_\bullet}{P} \qquad (5.2)$$

The uncertainties which exist in the measurement of the background, power monitor readings, and the counts (counting statistics) combine to give a total uncertainty in the transmission. The relationship can be found in Appendix III.

In principle, an additional correction should be made for small-angle scattering, that is, for neutrons which are scattered through small angles but nevertheless counted because of finite detector size. It is neglected because the detectors used subtend a solid angle of 10^{-4} steradian, and the spurious counts introduced will therefore be extremely small.

Multiple Scattering

The derivation of Equation 5.1 assumes that a neutron, once removed from the beam, is lost to it. This assumption is not justified, however, if the sample has

sufficiently large dimensions since additional deflections may possibly restore the neutron to the beam.

In this experiment, multiple scattering introduces negligible error because sample widths are much less than the neutron mean-free-path in palladium; horizontally-deflected neutrons therefore have extremely low probability of undergoing a second scattering before leaving the sample. Sample-heights are comparable with the mean free path, but the probability of a neutron undergoing two or more almost perfectly vertical deflections is again extremely small since this scattering is independent of azimuthal angle.

Microcrystalline Scattering and Extinction Effects

In order for the measured cross-section to be an atomic property, neutrons scattered from the beam must have been removed by interaction with the individual atoms. Removal caused by the grain or crystalline structure of the sample should be accounted for. Microcrystalline scattering, that is, coherent eleastic scattering from those members of the randomly oriented microcrystals which satisfy the Bragg reflection law, is a minor effect in this experiment since the operating energies were much above the cut-off energy for Palladium. The mechanics of this correction may be found in references (5) and (6). It must be modified, however, if grain alignment occurs.

Extinction effects,[6] which result from a lack of illumination of the crystal grains by the neutron beam caused by Bragg reflection from preceeding grains, are a minor source of error in the cross-section, and no correction is performed.

Impurities

The experimental cross-section obtained by Eq. 4.1 can be shown to be a weighted sum of cross-sections of the various substances comprising the sample. If n_{Pd}, n_1, ...n_k are the number of atoms per unit volume of palladium and elements 1, 2, ...k, then the true palladium cross-section is given by

$$\sigma_{Pd} = \frac{1}{n_{Pd} t} \ln \left(\frac{1}{T} \right) - \sum_{i=1}^{k} \frac{n_i}{n_{Pd}} \sigma_i \qquad (5.3)$$

The percentage impurities in our sample were obtained by a spectroscopic analysis from which the ratios n_i/n_{Pd} were calculated. Approximate values for the σ_i were obtained from BNL 325. The correction for impurities was much less than that due to counting statistics, and was consequently not performed.

SECTION VI

RESULTS

In measuring the neutron cross-section, two separate samples were employed: a thick ($\sim$2 cm.) sample having dimensions of .802" $\pm$ .002" x 1.165" $\pm$ .001" x .0505" $\pm$ .005" and a thin ($\sim$.5 cm.) sample having dimensions of .200" $\pm$ .001" x 1.165" $\pm$ .001" x .0495" $\pm$ .005". Because the cross-section uncertainty is inversely proportional to the sample thickness (see Eq. A3.11), the thin sample gives good cross-section results only at resonances. The values obtained between resonances for this run are consequently not contained in the final plot. The sample density was measured to be 12.2 g/cm^3, in good agreement with the published value[9]. Rotor speed measurements were taken frequently and showed small fluctuations about the mean values. The polyethylene drift-tubes were checked regularly to ensure their full inflation.

Background readings taken periodically showed a value of 13 counts per hour (for an 8 μsec. channel width) and were constant over the running period. The background comprised 10 to 20 percent of the total data counts, and its uncertainty is one of the principal sources of error in the experiment.

In evaluating the data, a collection time of .5 μsec. and a delay uncertainty (see Section III) of 4 μsec. are used. The total time uncertainty, due principally to the channel width and burst width, was found to be 11 μsec. for the 3000 r.p.m. runs, and 40 μsec. for the 850 r.p.m. run. The instrument resolution for the two rotor speeds are respectively .43 and 1.53 μsec/meter; the neutron energy uncertainty dE is proportional to the instrument resolution, and varies as $E^{3/2}$. Figure 3 contains a plot of the total energy uncertainty as a function of both rotor speed and neutron energy.

Three series of measurements were performed: both samples were employed at 3000 r.p.m. while only the thick sample was used at 850 r.p.m. This low speed run was made in order to determine the cross-section in the lower energy regions. A predetermined number of neutron bursts terminated the counting for each run. A tabulation of the run parameters may be found in Table 2.

Cross-Section Uncertainty

The total uncertainty in cross-section is approximately 20 percent away from resonances, and 10 percent at resonances. The following factors contribute to the overall cross-section uncertainty:

background uncertainty	7.5 percent
statistics	13.0 percent

sample nonuniformity	.1 percent
impurity contamination	1.0 percent
rotor speed variation	.1 percent
coherent and multiple scattering	< 1.0 percent
uncertainty in power normalization	< .01percent

As indicated before, the background counts and the counting statistics are the principal sources of uncertainty.

Cross-Section Data

Appendix VI presents the data in analyzed form. A plot of the experimentally obtained neutron cross-section has been obtained from this data and is presented in Graph 1, which is found on page 29. Maximum accuracy in the energy ranges from .07 to 2.0 e.v. and from 2.0 to 10.0 e.v. were obtained employing the thick samples at 850 r.p.m. and 3000 r.p.m. respectively. As previously described, the 3000 r.p.m. run employing the thin sample was used only to define the resonances at 2.97 e.v., 12.0 e.v., and 13.1 e.v. because of its relatively poor accuracy elsewhere.

Inspection of Graph 1 shows that the cross-section values obtained for the two thick sample runs agree within experimental accuracy. A new resonance of 14.3 ± 1.6 barns was found at an energy of $2.97 \pm .06$ e.v. Doppler broadening introduces an additional .05 e.v. energy uncertainty at resonance, resulting in a total energy uncertainty of .07 e.v. in the resonance location.

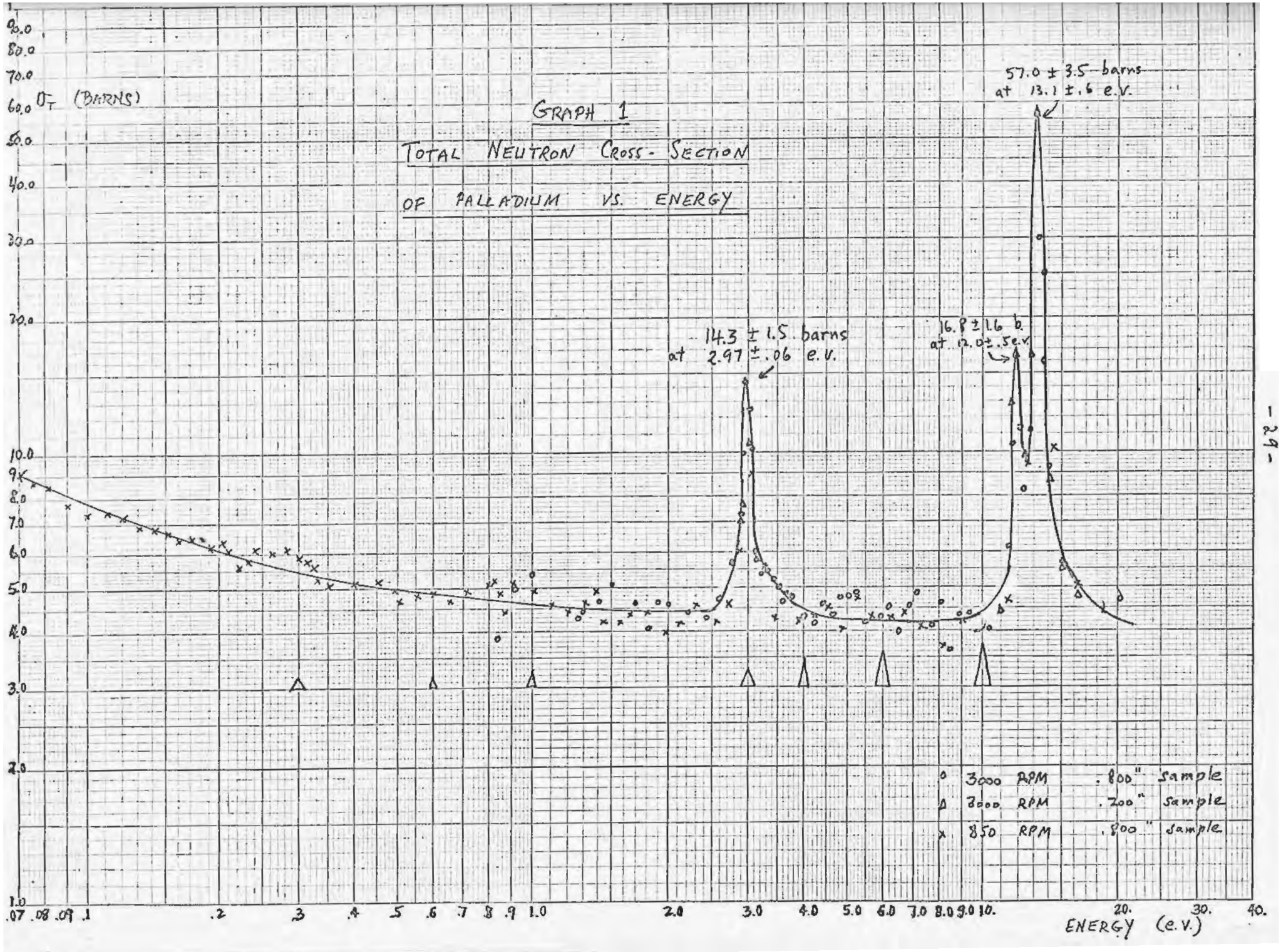
GRAPH 1
TOTAL NEUTRON CROSS-SECTION
OF PALLADIUM VS. ENERGY
σ_T (BARNS)
57.0 ± 3.5 barns
at 13.1 ± .6 e.v.
14.3 ± 1.5 barns
at 2.97 ± .06 e.v.
16.8 ± 1.6 b.
at 12.0 ± .5 e.v.
○ 3000 RPM .800" Sample
△ 3000 RPM .200" Sample
× 850 RPM .800" Sample
ENERGY (e.v.)

The measured resonances of 16.8 ± 1.7 barns at 12.0 ± 6 e.v. and 57 ± 3.6 barns at 13.1 ± .6 e.v. fail to agree with previously measured values[1] by a factor of two. This discrepancy is attributed to the energy-smearing effect introduced by the wide channels employed in our experiment; the 0.6 e.v. energy width of the 8 μsec. channel at resonance is much greater than the .15 e.v. half-widths Γ reported for these resonances. However, this energy smearing should not appreciably affect the cross-section at the 2.97 e.v. resonance since the .06 e.v. channel width there is less than .10, a reasonable assumption for Γ.

Improvement of Accuracy

Because the burst width is the principal source of timing uncertainty, the energy resolution can be improved by decreasing the rotor speed. However, since the rotor transmission drops considerably with increasing rotor speed (see Fig. 2 and Table 1 [open beam counting rates]), this would require open-beam, sample-intercepted, and background runs totaling approximately 50 hours if 3 percent statistics are desired. This would require making the apparatus more automatic.

The accuracy of cross-section measurement is limited principally by statistical errors introduced by low count rates. More counts can be obtained by longer runs, but

~~but~~ since the accuracy increases as the square root of the running time, a sizeable increase in accuracy would again require making the equipment automatic. Lower rotor speeds, another method of increasing the accuracy, will increase the counting rate, but only at the expense of poorer energy resolution, as described above. The second principal source of cross-section error is the uncertainty in background, and may be reduced by better shielding of the equipment and detectors. This error would also be made negligible by higher count rates.

Two suggestions for achieving higher count rates which do not entail longer counting times are the installation of a fuel element closer to the chopper reactor port, and the employment of more efficient neutron detectors.

APPENDIX I

CORRECTION FOR DEAD-TIME COUNTING LOSSES

The dead-time of the multichannel analyzer, that is, the time after receiving a pulse during which the analyzer is inoperative, is 16 μsec. The following method allows us to correct for the pulses which were missed. Let

RC_i = number of recorded counts in the i^{th} channel

C_i = true number of pulses incident upon the i^{th} channel

B = number of bursts

$n = \frac{16\mu sec}{\text{channel width}}$ = number of channels rendered inoperative by dead-time

PO_i = observed probability of receiving, during one burst, one or more counts in the i^{th} channel

P_i = true probability of receiving, during one burst, one or more counts in the i^{th} channel

The counting rates are sufficiently low that the probability of receiving two or more neutrons per burst in any channel is negligible in comparison with the probability of receiving one neutron per burst in that channel.*

---

*This statement follows from the incoming counts obeying Poisson statistics. The probability of receiving n counts per burst in channel i is

$$P_i(n) = \frac{N_i^n \, e^{-N_i}}{n!} \qquad (A1.1)$$

where N_i is the average number of counts received per burst. N_i therefore satisfies the equation $N_i = C_i/B$ and is typically on the order of 10^{-2}. The probability of receiving two or more counts per burst is, by (A1.1)

$$P_i(2) + P_i(3) + \ldots = [N_i/2! + N_i^2/3! + N_i^3/4! + \ldots]P_i(1) \qquad (A1.2)$$

or less than 10^{-3} times the probability of receiving one count per burst.

To an excellent approximation, therefore P_i and PO_i may be interpreted as the probabilities of receiving and recording one count per burst in the i^{th} channel, and losses due to two or more simultaneous counts in one channel will be assumed negligible.

The probability PO_i of actually recording a count in the i^{th} channel is the product of the probability P_i that a count was received in the i^{th} channel and the probability $P(\bar{A}_{i-1}, \bar{A}_{i-2}, \ldots, \bar{A}_{i-r})$ that no counts were recorded in the preceeding r channels, where

$$r = i-1 \qquad \text{for} \qquad i \leq n$$

$$r = n \qquad \text{for} \qquad i > n$$

A_j here represents the event that a count was recorded in the j^{th} channel and a bar indicates the complementary event. PO_i may be split into such a product because the arrivals, per burst, of counts at different channels are statistically independent of one another.

The above result may be simplified by using the well-known formula

$$P(\bar{A}_{i-1}, \bar{A}_{i-2}, \ldots, \bar{A}_{i-r}) = 1 - \left[\sum_{j=i-1}^{j=i-r} P(A_j)\right] + \left[\Sigma \text{ all allowed double probabilities } P(A_j, A_k)\right] \ldots \qquad (A1.3)$$

Any double or higher order probability $P(A_j, A_k, A_l, \ldots)$ must vanish, since it represents the probability of recording during

one burst neutrons in channels j, k, ℓ, ... less than n apart. Therefore

$$PO_i = P_i \left[1 - P(A_{i-1}) - P(A_{i-2}) - \ldots - P(A_{i-r})\right] \qquad (A1.4)$$

$P(A_i)$ is the probability per burst of recording a count in the i^{th} channel, and so is equal to PO_i. By multiplying both sides by B^2, the above equation can be cast into the form

$$C_i = \frac{B}{B - C_{i-1} - C_{i-2} - \ldots - C_{i-r}} \, RC_i \qquad (A1.5)$$

where $r = n$ if $i > n$

$r = i-1$ if $i \leq n$

This is the formula used to correct for the dead-time counting losses.

APPENDIX II
FORTRAN PROGRAM

```
    XEQ
    LIST
    DIMENSION   CA1(256), CB1(256),  CA2(256),  CB2(256), CA3(256),
   C CB3(256),  DCA3(256),  DCB3(256),   DCA4(256),  DCB4(256),
   C CB5(256),  DCB5(256),
   C                TR(256),   DTR(256),  UNT(256),  CR(256),
   C  UNC(256),  DCR(256),  XNST(256),   TI(256),  E(256),  DE(256),
   CDEL(256),  UNE(256),                 X(256)
    NN1 = 1
    READ 520,  N1
  1 READ 520,  IMAX
520 FORMAT (I6)
     READ 500,  (CA1(I) , I = 1, IMAX)
     READ  500,  (CB1(I),  I = 1, IMAX)
500 FORMAT (12F6.0)
    READ  501,  BURA, BURB, FREQ,  POA,  POB,  T1,  LT4
501 FORMAT (6F10.1, I6)
     READ   504,  T2, T3,  T5,  T6,  DT6
504 FORMAT (3F10.5, 2F10.7)
    READ  505,  XL,  DXL,  DEN,  COF1
505      FORMAT (4F10.5)
    READ 520, NUM
     READ  520,  L
    READ 550, BACK, DBACK, POBACK
550 FORMAT (3F10.3)
     DENP =  (DEN)  *(T6)   * (2.54 )
    DT2 = ((T1)**2)     + ((T2)**2)  +  ((T3)**2)  + ((T5)**2)
     RAT  =  POA / POB
     RAT2 = ((RAT)**2)
     DRAT  =  (RAT + RAT2)  / POB
     RATT  =  ((DT6)/(T6))**2
     XLRAT = (DXL/XL) **2
     DT = SQRTF (DT2)
     XN =  5226.71 * XL **2
     COF  =  1.3422 * XL  * SQRTF  (COF1)
      DO 10  I = 1 , IMAX
     TI(I) = (T1)  *   (FLOATF((256)   * (LT4)  + I )  - 0.5)
```

```
      E(I) = XN/((TI(I))**2)
       UNE(I)  =    2. * SQRTF (XLRAT  +DT2/((TI(I))**2))
       DE(I)  =  (UNE(I)) * (E(I))
   10 DEL(I) = COF/ (TI(I))
      DEAD TIME CORRECTION
      CA2(1) = CA1(1)
      CB2(1) = CB1(1)
      SUMA = 0.
      SUMB = 0.
      DO 50 I = 2, NUM
      SUMA = SUMA + CA1(I - 1)
      SUMB = SUMB + CB1(I - 1)
      CA2(I) = BURA * (CA1(I) ) / (BURA - SUMA)
   50 CB2(I) = BURB * (CB1(I) ) / (BURB - SUMB)
      SUMA = SUMA + CA1(NUM)
      SUMB = SUMB + CB1 (NUM)
      NUMMM = NUM + 1
      DO 60  I  = NUMMM, IMAX
      CA2(I) = BURA * (CA1(I) ) / (BURA - SUMA)
      CB2 (I) = BURB * (CB1(I) ) / (BURB - SUMB)
      K  =  I  -  NUM
      SUMA = SUMA + CA1(I) - CA1(K)
   60 SUMB = SUMB + CB1(I) - CB1(K)
      BACKGROUND CORRECTION
       DO  200  I  = 1, IMAX
      CA3(I)= CA2(I) - BACK*POA/ POBACK
      DCA3(I) = DBACK* POA/ POBACK
      CB3(I) = CB2(I) - BACK* POB/ POBACK
      DCB3(I) = DBACK * POB/ POBACK
       IF (CA3(I))  250,250,251
  250 CA3(I) = 1.0
  251 IF (     CB3(I))  260,260,261
  260 CB3(I) = 10000000.
  261 SQDCB4   = CB3(I) + DCB3(I)**2
      DCB4(I) = SQRTF (SQDCB4   )
      DCA4(I) = SQRTF(CA3(I) + DCA3(I)**2)
      DCB5(I) = SQRTF(RAT2*SQDCB4    + DRAT*CB3(I)**2)
      CB5(I) = RAT * CB3(I)
      TR(I) = (CB5(I)) / CA3(I)
      UNT(I) = SQRTF (((DCB5(I)) / (CB5(I))) ** 2 + ((DCA4(I)) /
     C (CA3(I))) ** 2)
```

```
      DTR(I) = UNT(I) * TR(I)
      XNST(I) = - LOGF  (TR(I))
      CR(I) = (XNST(I)) / DENP
      UNC(I) = SQRTF (RATT + ((UNT(I)) / (XNST(I))) ** 2)
      DCR(I) = (CR(I)) * (UNC(I))
  200 CONTINUE
      PRINT 599
  599 FORMAT (30H1 FAST CHOPPER DATA REDUCTION    )
      PRINT 600
  600 FORMAT (                          5H POA 9X, 5H POB 9X, 4H T1 10X,
     C4H T2 10X, 4H T3 10X, 4H T5 )
      PRINT 601,  POA, POB,  T1,  T2,  T3,  T5
  601 FORMAT  ( 1X,  3(F12.1,  2X),  3(F12.5,  2X))
      PRINT 602
  602 FORMAT (8H0 FREQ   6X, 5H LT4 5X, 4H T6 10X, 5H DT6 9X,
     C  4H XL 10X,  5H DXL 9X)
      PRINT 603,  FREQ,  LT4,  T6,  DT6,  XL,  DXL
  603 FORMAT (1X ,    F12.1, 2X, I8, 2X,  2(F12.7,2X), 2(F12.5, 2X))
      PRINT 606
  606  FORMAT (7H0 BURA  9X, 6H BURB 10X, 6H DENP 9X, 5H DT2 10X,
     C5H RAT 8X)
      PRINT 607, BURA, BURB, DENP, DT2, RAT
  607 FORMAT (1X, 2(F13.0,3X),F12.5,3X,F12.2, 3X,   F10.4, 3X)
      PRINT 622
  622 FORMAT ( 6H0 BACK 7X, 7H DBACK 6X, 8H POBACK  5X, 5H DEN  5X,
     C6H COF1  )
      PRINT 623, BACK, DBACK, POBACK, DEN, COF1
  623 FORMAT (F10.1, 4X, F10.1, 4X, F10.1 4X, F12.5, 4X, F12.5)
      PRINT 608
  608 FORMAT (8H0 XLRAT  5X, 4H XN 9X, 5H COF 8X, 5H NUM 3X, 4H DT
     C 5X, 6H IMAX    )
      PRINT  609,  XLRAT,  XN,  COF,  NUM,  DT , IMAX
  609 FORMAT (1X, F10.6, 3X, 2(F10.5, 3X), I6, 3X, F12.2, I6)
      PRINT 599
      PRINT 612
  612 FORMAT (3H0 I 5X, 8H CA1(I) 6X, 8H CA2(I) 7X, 8H CA3(I) 7X,
     C9H DCA3(I) 6X, 9H DCA4(I) 6X)
      PRINT 613, (I,CA1(I), CA2(I), CA3(I), DCA3(I),DCA4(I),
     C I = 1, IMAX)
  613 FORMAT (1H I6, 2X, F10.1,  4X, F11.2, 4X, F11.2, 4X, F11.2,
     C  4X, F11.2)
```

```
      PRINT 599
      PRINT 614
  614 FORMAT (3H0 I 5X, 8H CB1(I) 6X,                  8H CB3(I) 7X,
     C 9H DCB3(I) 6X, 9H DCB4(I) 6X, 8H CB5(I) 12X, 9H DCB5(I) )
      PRINT 615,  (I,CB1(I),          CB3(I), DCB3(I), DCB4(I), CB5(I),
     CDCB5(I), I=1, IMAX)
  615 FORMAT (1H I6, 2X, F10.1,  4X,              F11.2, 4X, F11.2,
     C  4X, F11.2, 4X, F17.5,  3X, F17.5)
      PRINT 599
      PRINT 616
  616 FORMAT (3H0 I 3X, 7H TI(I) 9X,                  7H DE(I) 8X,
     C 6H E(I) 9X, 7H TR(I) 8X,8H DTR(I) 7X, 8H UNT(I) )
      PRINT 617, (I, TI(I),          DE(I), E(I), TR(I), DTR(I), UNT(I),
     C I = 1 , IMAX)
  617 FORMAT (1H I6, 5X, F11.2,              5X, F10.3, 5X, F10.3,
     C 5X, F10.7, 5X, F10.7,  5X, F10.4)
      PRINT 599
      PRINT 618
  618  FORMAT (3H0 I 8X,                 8H UNE(I) 7X, 7H DE(I) 8X,
     C 6H E(I) 9X, 7H CR(I) 8X, 8H DCR(I) 7X, 8H UNC(I) )
      PRINT 619, (I,          UNE(I), DE(I), E(I), CR(I), DCR(I), UNC(I),
     C I = 1, IMAX)
  619 FORMAT ( 1H I6,               5X, F10.4, 5X, F10.3, 5X,F10.3,
     C 5X, F10.3, 5X, F10.3,5X, F10.4  )
      PRINT 599
      PRINT 620
  620  FORMAT (3H0 I 8X, 6H E(I) 9X, 7H DE(I) 8X, 8H DEL(I) 22X,
     C 9H XNST(I) )
      PRINT 621, (I, E(I), DE(I), DEL(I), XNST(I), I = 1, IMAX)
  621 FORMAT( 1H I6, 5X, F10.3, 5X, F10.3, 5X, F10.3,20X, F12.6)
      PRINT 650, (NN1, N1)
  650  FORMAT (18H JUST FINISHED NO  I6, 4H OF I6, 6H DECKS )
      IF (L)  998,998,999
  999 CALL FLIP (5HM1446)
       PUNCH   599
       PUNCH  600
      PUNCH 601,  POA, POB,  T1,  T2,  T3,  T5
       PUNCH 602
      PUNCH 603,  FREQ,  LT4,  T6,  DT6,  XL,  DXL
      PUNCH  606
      PUNCH 607, BURA, BURB, DENP, DT2, RAT
```

```
      PUNCH  622
      PUNCH 623, BACK, DBACK, POBACK, DEN, COF1
       PUNCH 608
      PUNCH  609,  XLRAT,  XN,  COF,  NUM,  DT , IMAX
      PUNCH  599
      PUNCH  612
      PUNCH 613, (I,CA1(I), CA2(I), CA3(I), DCA3(I),DCA4(I),
     C I = 1, IMAX)
       PUNCH   599
      PUNCH  614
      PUNCH 615,  (I,CB1(I),          CB3(I), DCB3(I), DCB4(I), CB5(I),
     CDCB5(I), I=1, IMAX)
       PUNCH   599
       PUNCH  616
      PUNCH 617, (I, TI(I),          DE(I), E(I), TR(I), DTR(I), UNT(I),
     C I = 1 , IMAX)
         PUNCH  599
       PUNCH  618
      PUNCH 619, (I,         UNE(I), DE(I), E(I), CR(I), DCR(I), UNC(I),
     C I = 1, IMAX)
         PUNCH  599
       PUNCH  620
      PUNCH 650, (NN1, N1)
  998 CONTINUE
    . NEW BATCH OF CARDS
      NN1 = NN1 + 1
      IF (NN1 - N1)  1, 1, 1000
 1000 CALL EXIT
      END
```

APPENDIX III

DISCUSSION OF DATA ANALYSIS

This appendix describes the method of data analysis performed by the IBM 709 computer, employing the same notation as that used in the Fortran Program.

The letters A and B refer respectively to the open-beam and sample-intercepted runs. The channel number I ranges from 1 to 255. The number of bursts are denoted by BURA and BURB, the power monitor readings are POA and POB, and the raw data consists of the sets of counts CA1 (I) and CB1 (I) which are first corrected for dead-time counting losses by equation A1.5, yielding CA2 (I) and CB2 (I).

A run for background counting rate with a power monitor reading POBACK has an average number of counts per channel BACK $\pm$ DBACK. The same channel-width, frequency, and delay-time are used for runs A and B as for the background run so that the true counts may be obtained from CA2 and CB2 by subtracting from them the counts BACK, normalized to equal power. That is, the background-corrected counts are CA3 (I) $\pm$ DCA3 (I) and CB3 (I) $\pm$ DCB3 (I), where

$$CA3\ (I) = CA2\ (I) - [BACK]\cdot[POA/POBACK] \qquad (A3.1)$$

$$DCA3\ (I) = [DBACK]\cdot[POA/POBACK] \qquad (A3.2)$$

Similar formulae hold for run B.

An additional uncertainty in counts results from statistical errors. Open beam counts CA3 (I) $\pm$ DCA3 (I) become CA3 (I) $\pm$ DCA4 (I) where

$$DCA4\ (I) = \sqrt{(DCA3\ (I))^2 + CA3\ (I)} \qquad (A3.3)$$

The first term under the radical gives the uncertainty in background, while the second gives the $\sqrt{CA3\ (I)}$ uncertainty in the number of counts CA3 (I). A similar formula is used to obtain CB3 (I) $\pm$ DCB4 (I).

Run B is then normalized to equal power with A, giving rise to counts CB5 (I) $\pm$ DCB5 (I). The normalization relationship is given by

$$CB5\ (I) = [CB3\ (I)] \cdot [POB/POA] \qquad (A3.4)$$

and

$$DCB5\ (I) = \sqrt{[(POB/POA)(DCB4\ (I))]^2 + (CB3\ (I))^2[(POB/(POA)^2 + (POB^2/POA)^2]}$$

where the first term under the radical is the uncertainty in counts resulting from the uncertainty in background, and the second is the uncertainty in counts resulting from the uncertainty in the power ratio POB/POA.

The transmission TR (I) $\pm$ DTR (I) and its fractional uncertainty UNT (I) at the I^{th} channel are then obtained from the formulae

$$TR\ (I) = CB5\ (I)/CA3\ (I) \qquad (A3.6)$$

$$UNT\ (I) = \sqrt{[DCB5\ (I) / CB5\ (I)]^2 + [DCA4\ (I) / CA3\ (I)]^2} \quad (A3.7)$$

and

$$DTR\ (I) = (TR\ (I)) \cdot (UNT\ (I)) \quad (A3.8)$$

Then $n\sigma t$ is obtained from

$$XNST\ (I) = -\ln TR\ (I) \quad (A3.9)$$

The cross-section CR (I) $\pm$ DCR (I) in barns and its fractional uncertainty UNC (I) are obtained by use of the relationships

$$CR\ (I) = XNST\ (I)/DENP \quad (A3.10)$$

$$UNC\ (I) = \sqrt{(DT6/T6)^2 + (UNT\ (I)/XNST)^2} \quad (A3.11)$$

and the uncertainty in cross-section is DCR (I) given by

$$DCR\ (I) = [CR\ (I)] \cdot [UNC\ (I)] \quad (A3.12)$$

where DENP is 10^{-24} times the number of atoms per square centimeter of foil. The first term under the radical is the uncertainty in cross-section due to the uncertainty DT6 in the sample thickness T6, while the second is the uncertainty due to the uncertainty in measurement of the transmission.

Also computed are the mean time-of-flight TI (I) to the I^{th} channel and its uncertainty DT by formulae (A3.13) and 5.2 respectively.

$$TI\ (I) = [T1] \cdot [256\ (LT4) + I - (1/2)] \quad (A3.13)$$

where LT4 is the delay time and the 1/2 locates the time center of the channel. All times appear in microseconds.

The energy E (I) $\pm$ DE (I) and its fractional uncertainty UNE (I) are computed by formulae A3.14, A3.15, and A3.16

$$E\ (I) = 5226.71\ [XL]^2/[T\ (I)]^2 \qquad (A3.14)$$

$$UNE\ (I) = 2\ \sqrt{[DXL/XL]^2 + [DT/T\ (I)]^2} \qquad (A3.15)$$

$$DE\ (I) = [E\ (I)]\cdot[UNE\ (I)] \qquad (A3.16)$$

where XL $\pm$ DXL is the flight path length in meters and the numerical coefficient in (A3.14)is chosen so that E (I) and DE (I) appear in e.v.

The Doppler width[7] DEL (I) in e.v. is computed from

$$DEL\ (I) = \sqrt{4kT(m/ME\ (I)} \qquad (3.17)$$

for comparison with the energy resolution DE (I) at the I^{th} channel. This uncertainty arises from thermal vibration (if a resonance occurs at channel I and if the target is treated as an ideal gas). Since noa priori knowledge is available about the location of resonances, DEL (I) cannot be combined with DE (I) to give an overall energy uncertainty.

APPENDIX IV

DETECTOR CAPTURE TIME

Consider only neutrons of velocity v entering the detector bank at time t = 0 and longitudinal position x = 0. If the detectors have length L and mean free path λ for neutrons with this velocity, then the probability of neutron capture between x and x + dx for those neutrons which <u>are</u> captured is

$$P(x)\,dx = \frac{e^{-x/\lambda}\,dx/\lambda}{\int_0^L e^{-x/\lambda}\,dx/\lambda} \qquad (A4.1)$$

The mean capture distance and mean square capture distance at this velocity are

$$\bar{x} = \int_0^L x\,P(x)\,dx = \lambda\,\frac{1 - (1 + L/\lambda)\,e^{-L/\lambda}}{1 - e^{-L/\lambda}} \qquad (A4.2)$$

and

$$\overline{x^2} = \int_0^L x^2 P(x)\,dx = \lambda^2\,\frac{2 - [2 + 2L/\lambda + (L/\lambda)^2]e^{-L/\lambda}}{1 - e^{-L/\lambda}} \qquad (A4.3)$$

The mean capture time $\bar{t}$ and mean square capture time $\overline{t^2}$ are obtained by dividing the above capture distances by v and v^2.

The mean free path λ may be calculated as a function of neutron velocity v by means of the formula $\lambda = 1/n\sigma$ (A4.4)

where the number of atoms per c.c., n, is computed from

$$n = P/kT \qquad (A4.5)$$

Here, the BF_3 is assumed to be a perfect gas at pressure P. The dependance of σ, the ${}_5B^{10}$ (n,α) ${}_3Li^7$ reaction cross-section, on the neutron velocity can be found in reference 8. An effective detector length, L, of 8.9 cm. is used.

The results of the above calculations are tabulated below. Δx and Δt, respectively, root-mean-square capture distance and time, are given in the following table:

$E_{e.v.}$	$\bar{x}/L$	$\Delta x/L$	$\bar{t}$(μsec.)	Δt(μsec.)
.0624	.49	.28	12	6.9
1.0	.49	.28	3.1	1.8
6.25	.50	.29	1.3	.8

The numerical values show that, to a good approximation in the energy range 0.1 to 10 e.v., the average capture distance $\bar{x}$ is half of the detector length, and the standard deviation of the capture distance is three-fourths of the average capture distance. Similarly, the average capture time is half of the time required to traverse the detector, and the standard deviation is three-fourths of the traversal time.

The path difference to various transverse portions of the detectors is calculated using a flight-path of 25.83

meters and a detector height of 18 inches. The maximum flight-path difference is found to be one-fifth inch, much less than the uncertainty of .3L due to longitudinal path differences.

APPENDIX V

SPECTROSCOPIC ANALYSIS

A spectroscopic analysis of the palladium metal sample employed was performed by the Cabot Spectrographic Laboratory. The results of this analysis showed that the following impurities were present in the amounts indicated:

Rhodium	10-100 p.p.m. (by weight)
Platinum	50-500 p.p.m.
Iridium, Osmium, Rhenium	< 100 p.p.m.
Ruthenium	< 10 p.p.m.

Impurities Estimate

The cross-section of platinum is flat and would contribute $\sim .002$ barns for a maximum impurity of 0.03 percent by weight. Observation of abrupt changes in the transmission curves occuring at energies where well-formed resonances of the other metals of the family occur permits estimation of the percentage impurity. Using Eq. A5.1 for the observed transmission,

$$T = \exp\left[- t n_{Pd}\left(\sigma_{Pd} + \sum_{A \neq Pd} \alpha_A \sigma_A\right)\right] \qquad (A5.1)$$

where σ_{Pd} = true cross-section

t = thickness of sample

n = no. atoms/volume

A = nuclide other than Pd.

$\alpha_A = n_A/n_{Pd}$

including the effects of impurities, and using changes in the transmission discussed above, it is possible to assert that the impurities exist in lesser amounts than the following percentages:

Rhodium, Rhenium	.01 Percent
Osmium	.04 Percent
Iridium	.02 Percent

These estimates, although coarse, do provide an upper bound for the uncertainties involved.

APPENDIX VI

IBM COMPUTER OUTPUT

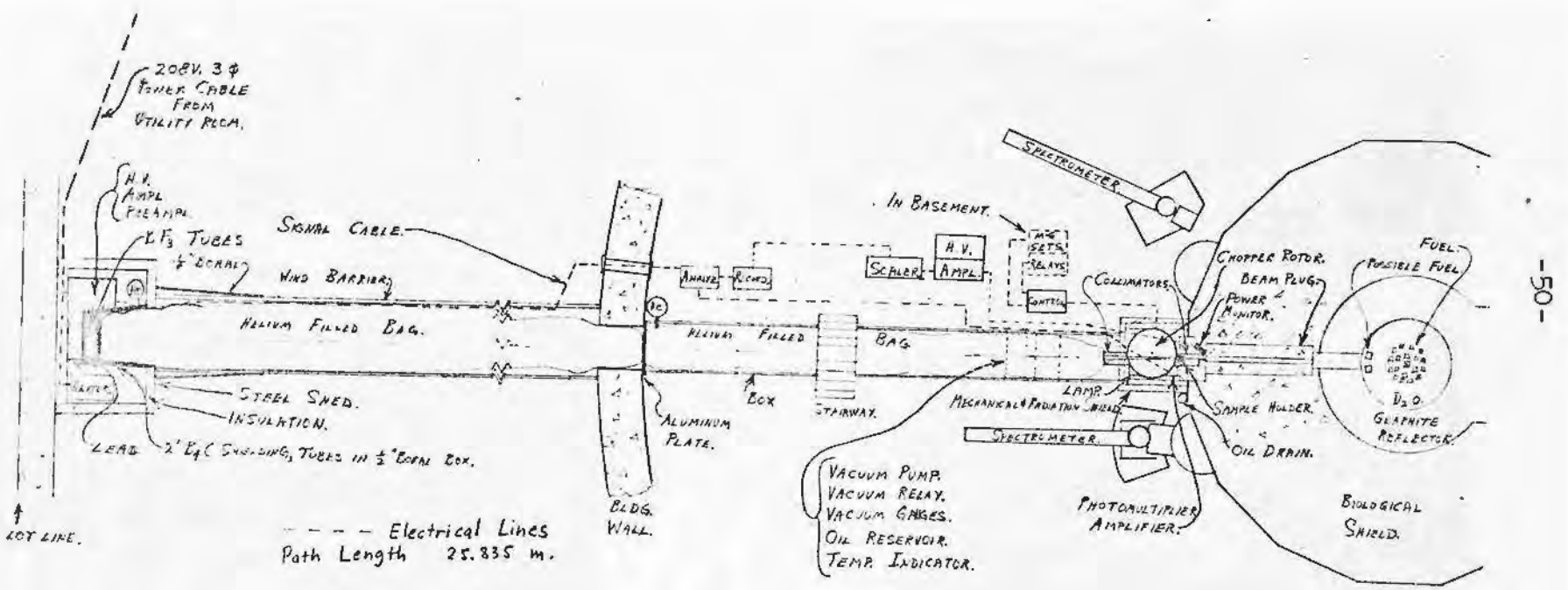
208V. 3φ
Power Cable
From
Utility Room.
H.V.
Ampl
Preampl.
BF_3 Tubes
4" Bore
Signal Cable.
Wind Barrier
Helium Filled Bag.
Steel Shed.
Insulation.
Lead
2" B_4C Shielding, Tubes in ½" Boron Box.
Lot Line.
Analyz
Record
Scaler
H.V.
Ampl.
In Basement.
Mtr Sets
Relays
Control
Spectrometer
Collimators.
Chopper Rotor.
Beam Plug.
Power Monitor.
Fuel.
Possible Fuel
Helium Filled Bag.
Box
Stairway.
Aluminum Plate.
Bldg. Wall.
Lamp.
Mechanical & Radiation Shield.
Spectrometer.
Sample Holder.
Oil Drain.
D_2O
Graphite Reflector.
Vacuum Pump.
Vacuum Relay.
Vacuum Gauges.
Oil Reservoir.
Temp. Indicator.
Photomultiplier Amplifier.
Biological Shield.
- - - - Electrical Lines
Path Length 25.835 m.

Fig 1

EXPERIMENTAL ARRANGEMENT ON REACTOR FLOOR

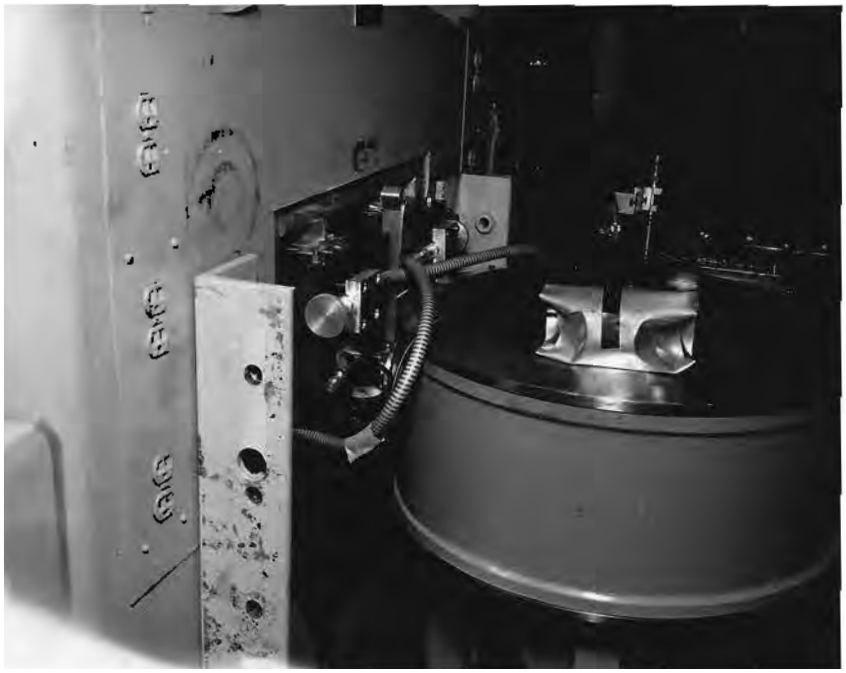

FAST CHOPPER

FLIGHT PATH

DETECTOR STATION

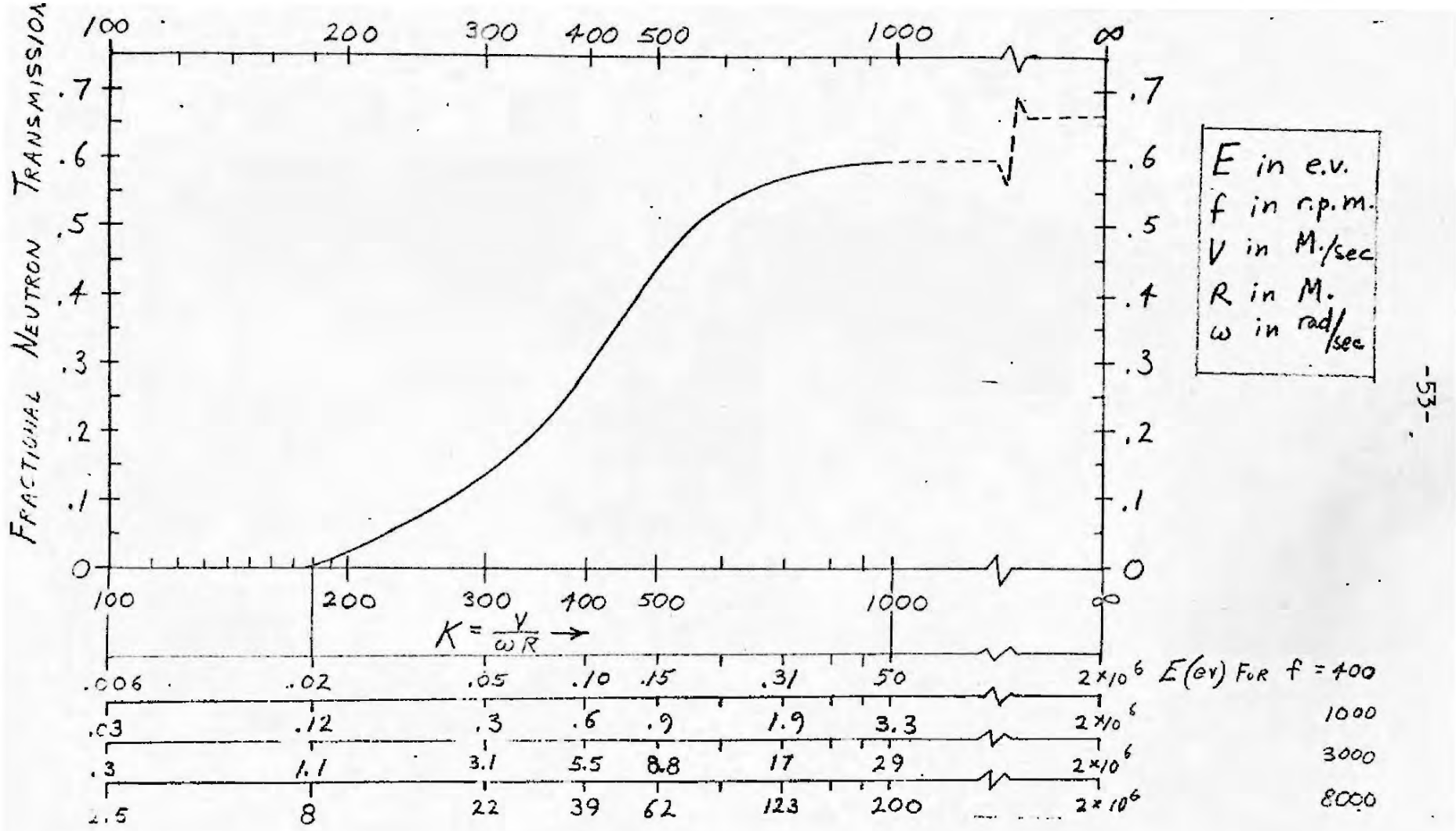
FRACTIONAL NEUTRON TRANSMISSION
100
200
300
400
500
1000
∞
.7
.6
.5
.4
.3
.2
.1
0
$K = \frac{V}{\omega R}$ →
.006
.02
.05
.10
.15
.31
50
2×10^6
E(ev) FOR f = 400
.03
.12
.3
.6
.9
1.9
3.3
1000
.3
1.1
3.1
5.5
8.8
17
29
3000
2.5
8
22
39
62
123
200
8000
E in e.v.
f in r.p.m.
V in M./sec
R in M.
ω in rad/sec

FIG 2

RESOLUTION DETERMINED BY $\frac{\Delta E}{E} = -0.028 \frac{\Delta t}{M} \sqrt{E}$

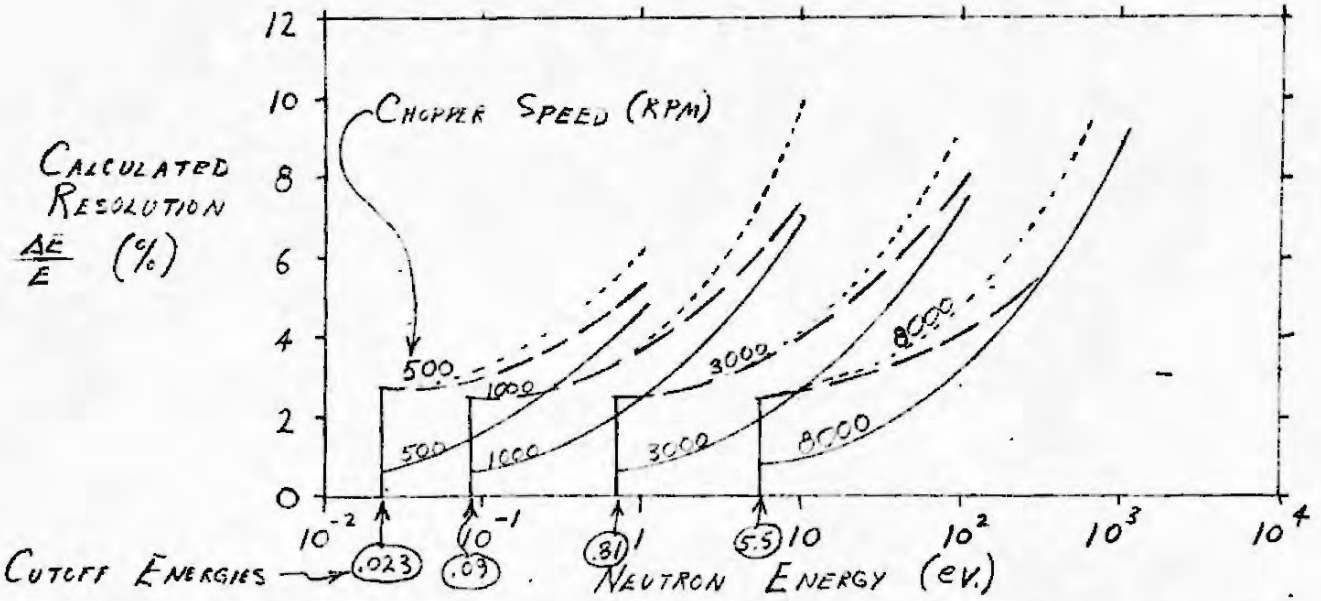

FIG. 3

KEY

—— DUE TO Δt OF CHOPPER SLIT ALONE.

—~— DUE TO Δt OF CHOPPER PLUS Δt CAUSED BY FINITE DETECTOR LENGTH (12").

..... DUE TO Δt OF CHOPPER PLUS Δt OF DETECTOR LENGTH PLUS Δt OF CHANNEL WIDTH PLUS 1 μSEC COLLECTION TIME.

f (RPM)	ANALYZER CHANNEL WIDTH
500	64 μSEC
1000	32 μSEC
3000	4 μSEC
8000	2 μSEC

TABLE 1

approx. rotor speed, r.p.m.	channel width, μs.	background per hour per channel	approx. open-beam counts per hour per channel	approx. counts per hour
400	64	12	1500	380,000
850	32	14	800	200,000
3000	8	13	95	24,000

Deck No	Power Monitor Reading	Sample Thickness	Uncert. in Samp Thickness	RPM	No. of Bursts	Channel Width (μsec.)	Burst Time (μsec)	Time of Run (hrs.)	Bkgnd. Counts	Pow. Mon. Bkgnd. Counts	Open Beam
1	24,892,000	.802"	.002"	3000	14,400,000	8	6.5	10			x
	24,940,00	.802"	.002"	3000	14,400,000	8	6.5	10			
								2	27±2	5,000,000	
2	24,892,000	.200"	.001"	3000	14,400,000	8	6.5	10			x
	24,603,000	.203"	.001"	3000	14,400,000	8	6.5	10			
								2	27±2	5,000,000	
3	26,143,000	.802"	.002"	850	4,080,000	32	23	10			x
	26,636,000	.802"	.002"	850	4,100,000	32	23	10			
								2	28±5	5,000,000	

TABLE 2

REFERENCES

1. Brookhaven National Laboratory Report, BNL 325 (Second edition, supplement 1), p. 78.

2. Carl Anderson, Ph.D. Thesis, M.I.T. Dept. of Nuclear Engineering, 1961

3. L.M. Bollinger, R.E. Coté and G.E. Thomas, A Critical Analysis of the Design and Application of Neutron Choppers, Proceedings of the Second United Nations International Conference on the Peaceful Uses of Atomic Energy; Geneva, 1958

4. Evans, The Atomic Nucleus (McGraw-Hill Book Company, Inc., New York, 1955)

5. E. Fermi, Nuclear Physics, University of Chicago Press, 1950, pp. 200-203.

6. D. Hughes, Pile Neutron Research, Addison-Wesley Publishing Co., Cambridge, Mass., 1953, pp. 268-272

7. Seidl, Hughes, Palevsky, Levin, Kato, and Sjostrand, Phys. Rev., 95, 485 (1954)

8. D. Halliday, Introductory Nuclear Physics, John Wiley and Sons, Inc., New York, 1955, p. 223

9. R. Leighton, Principles of Modern Physics, McGraw-Hill Publishing Co., Inc., New York, 1959, p. 728

10. Fermi, Sturm, and Sachs, Phys. Rev. 71 589 (1947)

11. Melkonian, Havens, and Rainwater, Phys. Rev., 92, 702 (1953)

12. Rosen, Desjardins, Rainwater and Havens, Phys. Rev., 118, 687 (1960)

13. Carter, Palevsky, Myers and Hughes, Phys. Rev., 92, 716 (1953)

14. Fermi and Marshall, Phys. Rev., 71, 666 (1947)

15. Moore, Miller, and Simpson, Phys. Rev., 118, 714 (1960)

16. Fluharty, Simpson, and Simpson, Phys. Rev., 103, 1778 (1956)

17. Simpson, Moore, and Simpson, Nuc. Sci, and Eng. 7, 187 (1960)

18. Vladimirski and Radlewich, Proc. Int. Conf. on Peaceful Uses of Atomic Energy, United Nations, New York, 1956, Vol. 18, paper 641

19. Weiss, Phys. Rev., 86, 271 (1952)